Cell Reports

Report

# Delta opioid receptors engage multiple signaling cascades to differentially modulate prefrontal GABA release with input and target specificity

## Graphical abstract

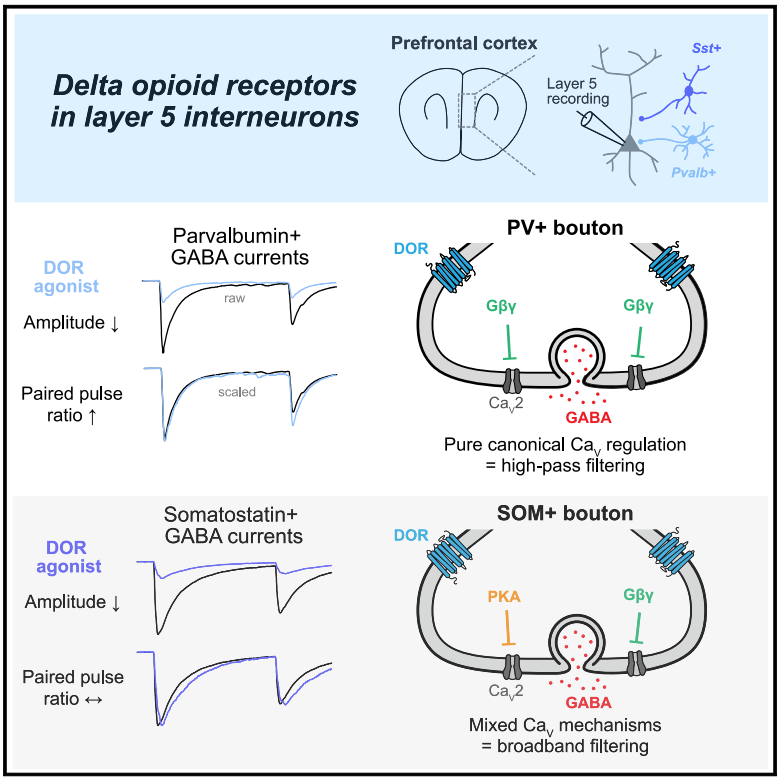


## Highlights

- Delta opioid receptors suppress transmission from parvalbumin and somatostatin cells
- DOR signaling in PV neurons engages canonical, Gβγ-dependent signaling
- SOM DOR engages two cascades in parallel, including $G_{i/o}$-independent mechanisms
- DOR signaling imposes different temporal filters on PV and SOM transmission

## Authors

Ryan P.D. Alexander, Kevin J. Bender

## Correspondence

ryan.alexander@ucsf.edu (R.P.D.A.), kevin.bender@ucsf.edu (K.J.B.)

## In brief

Opioids can influence neuronal activity by regulating transmitter release. Here, Alexander and Bender demonstrate that delta opioid receptors engage different mechanisms to regulate release from parvalbumin- and somatostatin-expressing interneurons in mouse prefrontal circuits, resulting in differential temporal filtering of inhibitory transmission depending on presynaptic cell identity.

Alexander & Bender, 2025, Cell Reports *44*, 115293
February 25, 2025 
https://doi.org/10.1016/j.celrep.2025.115293

CellPress

Cell Reports

CellPress
OPEN ACCESS

Report

# Delta opioid receptors engage multiple signaling cascades to differentially modulate prefrontal GABA release with input and target specificity

Ryan P.D. Alexander[1,2,*] and Kevin J. Bender[1,2,3,*]
[1]Weill Institute for Neurosciences, University of California, San Francisco, San Francisco, CA 94158, USA
[2]Department of Neurology, University of California, San Francisco, San Francisco, CA 94158, USA
[3]Lead contact
*Correspondence: ryan.alexander@ucsf.edu (R.P.D.A.), kevin.bender@ucsf.edu (K.J.B.)
https://doi.org/10.1016/j.celrep.2025.115293

## SUMMARY

Opioids regulate circuits associated with motivation and reward across the brain. Of the opioid receptor types, delta opioid receptors (DORs) appear to have a unique role in regulating the activity of circuits related to reward without liability for abuse. In neocortex, DORs are expressed primarily in interneurons, including parvalbumin- and somatostatin-expressing interneurons that inhibit somatic and dendritic compartments of excitatory pyramidal cells, respectively. But how DORs regulate transmission from these key interneuron classes is unclear. We found that DORs regulate inhibition from these interneuron classes using different G-protein signaling pathways that both converge on presynaptic calcium channels but regulate distinct aspects of calcium channel function. This imposes different temporal filtering effects, via short-term plasticity, that depend on how calcium channels are regulated. Thus, DORs engage differential signaling cascades to regulate inhibition depending on the postsynaptic target compartment, with different effects on synaptic information transfer in somatic and dendritic domains.

## INTRODUCTION

The opioid receptor family is comprised of three isoforms—mu, delta, and kappa—that are expressed throughout cortical and subcortical brain regions.[1–3] Although mu receptors are responsible for the main analgesic and addictive effects of opioid painkillers and narcotics,[4,5] delta opioid receptors (DORs) play a critical modulatory role in pain and reward circuitry.[6–8] While not habit forming on their own,[7] DORs contribute strongly to the development of reward associations. Indeed, DOR antagonists reduce conditioned place preference (CPP) for addictive drugs including morphine,[9–11] even though DORs cannot bind morphine themselves.[12] DORs are enriched in medial prefrontal cortex (mPFC),[13–15] where dysregulated opioidergic signaling is associated with impulsivity and drug-seeking behavior.[16,17] Remarkably, selective DOR knockdown in specific interneuron subpopulations in mPFC can prevent morphine-induced CPP.[18] Though DORs in mPFC, particularly in GABAergic interneurons, appear to have central importance in reward processing, how DORs regulate interneuron function remains unclear.

DORs primarily influence neuronal activity by modulating transmitter release from presynaptic terminals.[19,20] Canonically, DORs couple to $G_{i/o}$ signaling cascades.[21] Following receptor activation, $G\beta\gamma$ subunits dissociate from DORs and inhibit presynaptic voltage-gated calcium channels ($Ca_V$s)[22] by depolarizing the voltage dependence of channel activation.[23–25] This leads to a net reduction in intracellular Ca required for transmitter release and, thus, a reduction in vesicle release probability ($P_R$).[26,27] This style of neuromodulation is common across multiple $G_{i/o}$-coupled receptors, including presynaptic $GABA_B$, endocannabinoid, and catecholamine receptors.[28,29] Reductions in $P_R$ typically increase the relative amplitude of subsequent events, a process termed short-term synaptic facilitation. This form of short-term plasticity (STP) is due to the complex temporal dynamics of Ca in presynaptic boutons, Ca buffering mechanisms, and vesicle release proteins.[30] Presynaptic inhibition by G-protein signaling is ubiquitous throughout the brain and mostly results in increased STP.[28,29] However, at a variety of synapses, DORs and other opioid receptors appear to break this rule, inhibiting release with little to no increase in STP.[31–34] Why this occurs has remained largely unexplained.

Here, we studied DOR modulation in two subtypes of GABAergic interneurons that inhibit layer 5 (L5) pyramidal cells: parvalbumin-expressing (PV+) interneurons, which target the perisomatic regions, and somatostatin-expressing (SOM+) interneurons, which target dendritic regions, including apical dendrites that span the upper layers of cortex. We found that DORs suppressed GABA release in PV+ cells via canonical signaling pathways where $G\beta\gamma$ subunits alter the voltage dependence of activation of presynaptic $Ca_V$s, thereby reducing $P_R$ and increasing STP. By contrast, SOM+ cell transmission was regulated via multiple DOR-dependent signaling cascades engaged in parallel in the same bouton. DORs engaged both canonical $G\beta\gamma$-dependent modulation of $Ca_V$s and a second,

non-canonical pathway that was completely independent of $G_{i/o}$-based signaling. This second pathway also regulated presynaptic $Ca_V$s but through a reduction in $P_R$ without increasing STP—a mechanism recently described for dopaminergic regulation of glutamatergic transmission in mPFC.[35] These different forms of regulation at PV+ and SOM+ terminals thus produced differential suppression, or filtering, of GABA release that varied depending on the input frequency and inhibitory cell target. Taken together, these results show that DORs regulate inhibitory transmission in mPFC through multiple presynaptic mechanisms, even within a single axonal bouton of SOM+ interneurons. Further, this demonstrates that neuromodulators can engage multiple signaling cascades simultaneously to impose different temporal filtering rules depending on the target structure.

## RESULTS

### Unconventional regulation of prefrontal GABA release by DORs

DORs are highly expressed by GABAergic interneurons in mPFC, but how they regulate inhibitory transmission is not known. To test this, we made whole-cell recordings from L5 pyramidal cells in slices containing mPFC and evoked inhibitory postsynaptic currents (eIPSCs) with a bipolar stimulating electrode (Figure 1A). Application of the selective DOR agonist DPDPE (1 μM) reduced eIPSC amplitude (normalized amplitude [Norm Amp] = 0.47 ± 0.05, $n/N$ = 13/6; $p < 0.0001$; Figures 1B–1D). These effects were blocked by pre-treating slices with the DOR antagonist naltrindole (2 μM; Figure 1C). Deltorphin-II (1 μM), another agonist that displays preferential activation of type 2 DORs,[36] had comparable effects (Norm Amp = 0.41 ± 0.06, $n/N$ = 9/3; $p < 0.0001$), confirming that eIPSC reduction was mediated through DORs.

DORs, as with other opioid receptors, are commonly located presynaptically and reduce $P_R$ when activated.[9,27,37–39] Reduced $P_R$ increases variability in response amplitude, as measured by the coefficient of variance (CV), and typically increases short-term facilitation, as measured by the paired-pulse ratio (PPR). The PPR increased following DPDPE (Norm PPR = 1.11 ± 0.02; $p$ = 0.0024, Wilcoxon signed-rank test; Figure 1D), although the change was relatively modest (11% PPR increase vs. 53% amplitude decrease), whereas no significant change was observed with deltorphin-II (Norm PPR = 1.08 ± 0.04; $p$ = 0.13, Wilcoxon signed-rank test). Both DOR agonists reduced $CV^{-2}$ (Norm $CV^{-2}$; DPDPE = 0.64 ± 0.10; $p$ = 0.0031; deltorphin-II = 0.44 ± 0.09; $p$ = 0.0002; Figure 1G), indicating that DORs act presynaptically to decrease $P_R$. In agreement with this, DPDPE had no effect on postsynaptic membrane properties in these recording conditions where potassium channels are blocked by intracellular cesium (Figures S1B and S1C). In separate experiments using a $K^+$-based intracellular solution that does not block potassium channels, DPDPE modestly affected $R_{input}$, suggesting that DORs may have additional postsynaptic actions under physiological conditions.

Changes in $P_R$ often cause proportional reductions in response amplitude and increases in PPR.[40–42] By contrast, we observed what appeared to be relatively small increases in the PPR with DOR modulation. To determine whether this reflects unique release properties of mPFC GABAergic synapses or instead suggests that DORs modulate release without typical changes in STP, we benchmarked DOR modulation against manipulations that canonically affect $P_R$ or postsynaptic components of transmission. First, the external Ca concentration was reduced from 1.3 to 0.65 mM ("low Ca"), as this is known to reduce $P_R$. This reduced eIPSC amplitude and $CV^{-2}$ while causing an increased PPR (Figures 1D and 1G). To compare this to a purely postsynaptic form of neuromodulation, we blocked a fraction of $GABA_A$ receptors with gabazine (175 nM). This depressed the amplitude without altering the PPR or $CV^{-2}$ (Figures 1D and 1G). Of note, both manipulations were tuned to produce similar reductions in IPSC amplitude ($p$ = 0.55, one-way ANOVA; Figure 1D), allowing for a direct comparison to DOR-dependent modulation. When compared to these benchmarks, we found that DPDPE and deltorphin-II both resulted in less PPR changes than expected based on changing the external Ca concentration (DPDPE: $p$ = 0.038; deltorphin-II: $p$ = 0.017, Kruskal-Wallis test; Figure 1D) but clearly altered $CV^{-2}$, in sharp contrast to gabazine. To better visualize these differences, the Norm Amp and PPR in each condition were plotted as x-y coordinates with baseline values at (1.0, 1.0). This allowed us to quantify each amplitude-PPR relationship as a slope. Within this scheme, purely postsynaptic manipulations (e.g., gabazine) do not deviate from the x axis. By contrast, canonical forms of presynaptic modulation (e.g., low Ca) are depicted with a steep inverse relationship (Figure 1E). Surprisingly, both DPDPE and deltorphin-II exhibited slopes that were intermediate between both of these benchmarks (Figures 1E and 1F). These observations, coupled with the clear changes in $CV^{-2}$, suggest that DORs engage presynaptic signaling mechanisms that are difficult to explain at first sight.

### Differential DOR modulation of PV+ and SOM+ inputs

Electrical stimulation recruits GABAergic synapses independent of their source. Thus, one explanation for the mixed effects observed above is that DORs differentially filter transmission from different GABAergic inputs and the average of this is sampled with electrical stimulation of tissue. In neocortex, DOR-encoding *Oprd1* mRNA is expressed largely in PV+ and SOM+ cells[43,44] (Figure 2A). Therefore, we focused on release from these two cell classes. To test whether there is differential DOR regulation between PV+ and SOM+ afferents, we expressed channelrhodopsin-2 (ChR2) in either class using Cre-inducible vectors in PV- or SOM-Cre transgenic mice, respectively. Acute mPFC slices were taken 4–6 weeks post-injection, and optically evoked IPSCs (oIPSCs) were recorded in L5 pyramidal neurons (Figure 2B). Consistent with electrical stimulation and predictions from mRNA expression, the application of DPDPE suppressed both PV- and SOM-derived oIPSCs (Figures 2C and 2D). Although DPDPE increased the PPR in both subtypes (Norm PPR; PV = 1.32 ± 0.03; $p < 0.0001$; SOM = 1.08 ± 0.02, $p$ = 0.003), this change was far more modest for SOM- compared to PV-oIPSCs ($p < 0.0001$; Figure 2D). The amplitude-PPR slope for PV-oIPSCs was identical to that observed in low extracellular Ca ($p$ = 0.98, Holm-Sidak post hoc test; Figures 2E and 2F). By contrast, the SOM-oIPSC amplitude-PPR slope was shallower (SOM vs. low Ca: $p$ = 0.0026;

CellPress
OPEN ACCESS

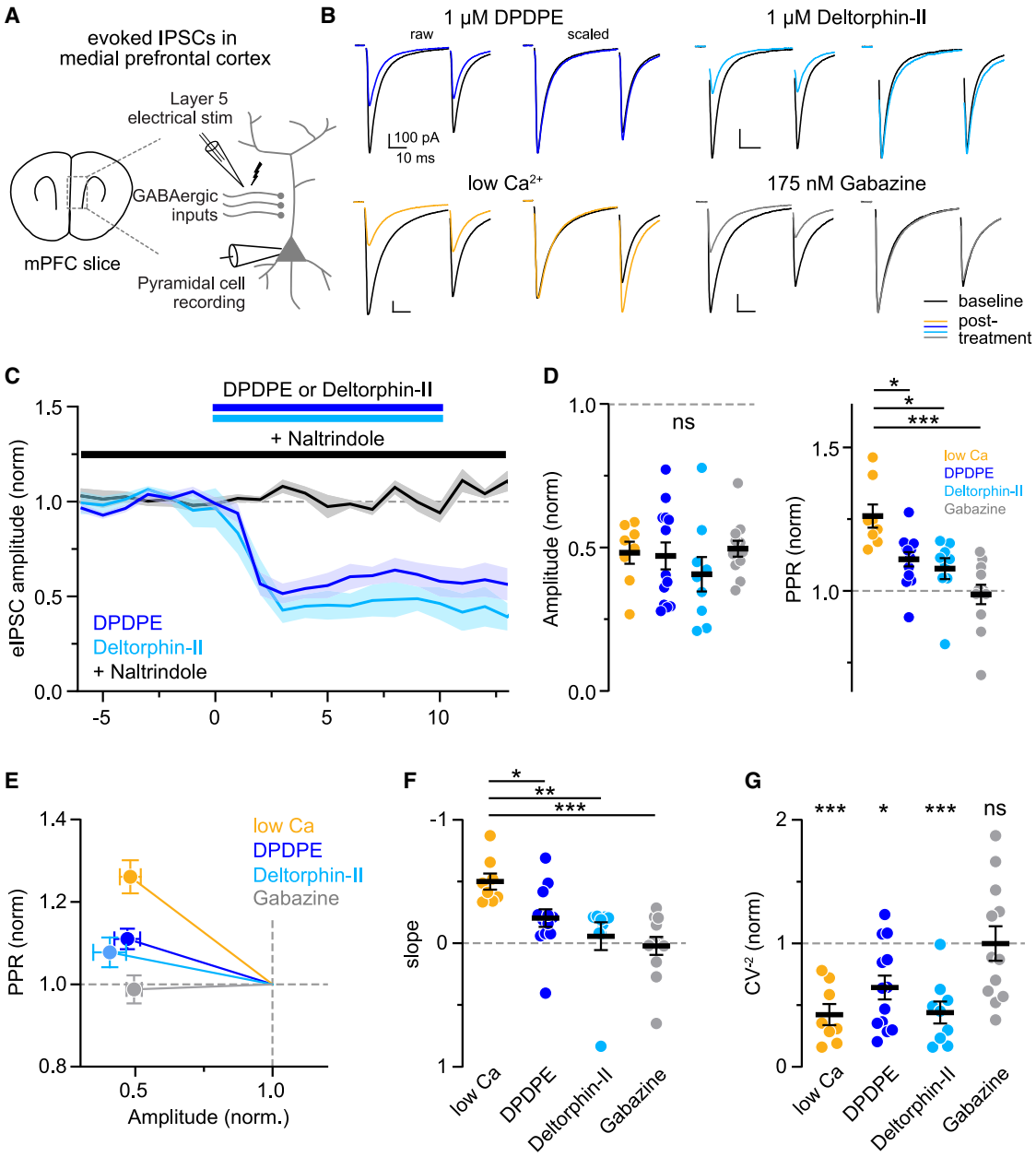


**Figure 1. DOR signaling suppresses inhibitory transmission onto L5 pyramidal neurons in mPFC**

(A) Schematic of experimental paradigm.

(B) Example current traces evoked by paired-pulse synaptic stimulation before and after application of DPDPE, deltorphin-II, gabazine, or low external Ca. Synaptic currents are overlaid as either raw values (left) or normalized to the first response (right) to visualize PPR differences. Scale bars depict 100 pA and 10 ms in all conditions.

(C) Summary time course plot of normalized eIPSC amplitudes during DOR agonist application (1 min bins).

(D) Summary plots of normalized eIPSC amplitude (left) and PPR (right) for all conditions.

(E) Plot of normalized PPR as a function of normalized eIPSC amplitude for each condition, with baseline at (1,1). Line slopes represent the degree of PPR change relative to the degree of amplitude change.

(F) Summary slope values for all conditions.

(G) Summary normalized $CV^{-2}$ for all conditions.

Colored circles represent individual cells, and black bars depict mean values ± SEM. *** $p < 0.001$; ** $p < 0.01$; * $p < 0.05$; ns, non-significant.

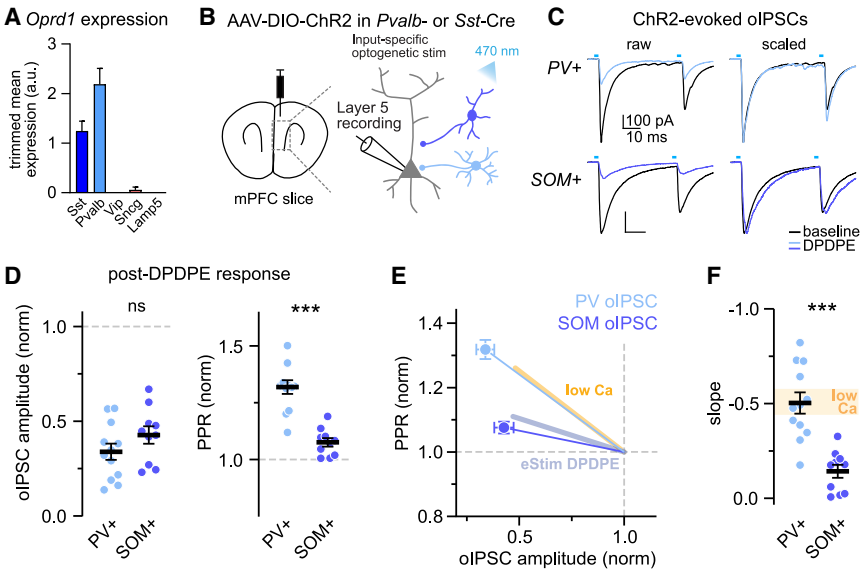


**Figure 2. GABA release from PV+ and SOM+ interneurons is differentially regulated by DORs**

(A) Expression of *Oprd1* mRNA across GABAergic cell classes from Allen Institute mouse patch-seq database.[43]

(B) Schematic depicting optogenetic stimulation paradigm.

(C) Example current traces of PV- (top) and SOM-derived (bottom) synaptic responses evoked by pairs of blue light-emitting diode (LED) flashes before and after DPDPE.

(D) Summary plots of normalized oIPSC amplitude (left) and PPR (right) between cell types.

(E) Normalized amplitude-PPR plot depicting slope relationships for PV- and SOM-oIPSCs after DPDPE, as well as for eIPSCs after DPDPE (blue line) and low Ca (yellow line) from Figure 1.

(F) Summary amplitude-PPR slopes for PV- and SOM-oIPSCs after DPDPE. The yellow bar depicts a low-Ca eIPSC slope for comparison.

Data are depicted as mean values ± SEM. *** $p < 0.001$; ns, non-significant.

SOM vs. PV: $p = 0.0008$, Holm-Sidak post hoc test; Figure 2F) and mirrored that observed with electrical stimulation. Taken together, these data suggest that DORs engage canonical signaling mechanisms at PV+ inputs, whereas effects observed at SOM+ inputs remain unexplained.

Recently, we described a form of presynaptic neuromodulation where $P_R$ is reduced without altering STP. At select excitatory inputs to mPFC pyramidal cells, the activation of $G_s$-coupled dopamine receptors (D1R or D5R, referred to collectively as D1R hereafter) suppressed glutamate release (i.e., lowered $P_R$) without an accompanying PPR increase.[35] This was termed "gain modulation" and was mediated by a form of protein kinase A (PKA)-dependent presynaptic $Ca_V$ modulation that increased the probability that the channel would fail to open at all in response to an action potential (AP). This contrasts with canonical Gβγ regulation, where channels still open in response to APs but do so only at more depolarized potentials relative to unmodulated states. When plotted as an amplitude-PPR slope, gain modulation resembles a postsynaptic effect and lies along the x axis. SOM+ DOR modulation is intermediate between both canonical and gain modulation forms of presynaptic regulation, suggesting that DORs do not utilize either mechanism exclusively. Therefore, we hypothesized that both processes are engaged in parallel in SOM+ terminals.

One prerequisite for this hypothesis, and gain modulation more broadly, is that $Ca_V$s must be coupled to release machinery in a "nanodomain" configuration where Ca influx from an individual $Ca_V$ is sufficient to trigger vesicular fusion. This configuration is common; most mature GABAergic synapses in hippocampus and cerebellum operate in a nanodomain configuration.[45,46] But whether release occurs via nanodomains in mPFC SOM+ and PV+ terminals remains unknown. This can be tested simply with divalent $Ca_V$ inhibitors. Manganese (Mn) and cadmium (Cd) are both divalents that block Ca permeation but do so with different dissociation rates. Mn dissociates quickly and mimics Gβγ-dependent canonical modulation by blocking and unblocking repeatedly during the duration of a single AP. By contrast, Cd dissociates slowly, blocking a single $Ca_V$ completely for the duration of a single AP.[47] Thus, Cd will mimic gain modulation if $Ca_V$s are coupled to release machinery in a nanodomain configuration.

To test the coupling configuration of mPFC interneurons, we applied external Mn or Cd and monitored L5 eIPSCs (Figures S2A–S2D). Both divalents suppressed eIPSC amplitude and $CV^{-2}$ dose dependently, but only Mn increased the PPR. Similar results were observed with PV- or SOM-specific oIPSCs. Cd decreased the amplitude in both cases without increasing the PPR (Figures S2E and S2F). Sub-saturating concentrations of Cd (5 μM) and Mn (100 μM) had little influence on single AP waveforms in either PV+ or SOM+ interneurons (Figures S2G–S2J), demonstrating that the main divalent effect on L5 IPSCs results from the blockade of presynaptic $Ca_V$. Ultimately, these data indicate that both PV+ and SOM+ terminals exhibit nanodomain configurations, opening the possibility that DORs engage non-canonical gain modulation in SOM+ terminals.

## PV+ interneurons exhibit canonical presynaptic $Ca_V$ inhibition

Before assessing the complexities of SOM+ terminals, we first wanted to validate that DORs engage exclusively canonical signaling cascades in PV+ terminals. DORs, like other opioid receptors, are classically coupled to inhibitory $G_{i/o}$ proteins[21,48] that inhibit presynaptic $Ca_V$s directly via translocated Gβγ subunits.[22,25,49–51] Since DOR modulation of PV-oIPSCs overlapped with the low-Ca relationship (Figures 2E and 2F), Gβγ-dependent $Ca_V$ inhibition presumably underlies the decrease in $P_R$,[27,28,48] as observed in hippocampal basket cells.[37] However, a recent study found that mu opioid receptors (MORs) suppress PV-oIPSCs in orbitofrontal cortex through cAMP-dependent PKA.[31] To test this in mPFC, we recorded PV-oIPSCs with the selective PKA inhibitor H89 (10 μM) included in the artificial

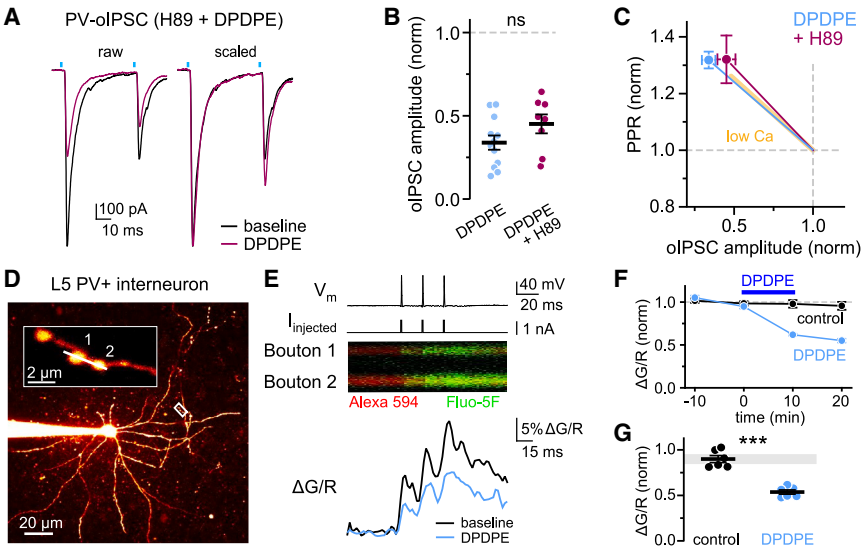


**Figure 3. DORs mediate canonical $Ca_V$ inhibition in PV+ interneurons**

(A) Example PV-oIPSC traces before and after DPDPE application with external H89.

(B) Summary normalized PV-oIPSC amplitudes.

(C) Summary amplitude-PPR plot depicting slope relationships of PV-oIPSCs after DPDPE. The low-Ca eIPSC relationship from Figure 1 is included for comparison (yellow line).

(D) z stack image of filled L5 PV+ interneuron. Imaging location (white box) is enlarged and rotated in the inset (top left). The line-scan region of interest (ROI) is represented as a white bar.

(E) Top: raw APs evoked by 1 ms step. Middle: superimposed Alexa 594 (red) and Fluo-5F (green) signals from boutons during high-frequency line scanning. Bottom: example Ca transients from ΔG/R fluorescence data at baseline and after DPDPE.

(F) Summary time course plot of normalized peak ΔG/R averaged over multiple PV+ cells for control and DPDPE conditions.

(G) Summary normalized peak ΔG/R in control and DPDPE conditions. Normalized ΔG/R data represent the final time point (20 min after DPDPE application) relative to the baseline average. Data are depicted as mean ± SEM. *** $p < 0.001$; ns, non-significant.

cerebrospinal fluid (ACSF) (Figure 3A). Application of H89 alone had no effect on L5 eIPSCs (Figures S3A and S3B), indicating that PKA did not regulate GABA release in mPFC under basal conditions. Following DPDPE, oIPSC depression was comparable to control (i.e., DPDPE alone; Figure 3B), as was the amplitude-PPR relationship ($p$ = 0.73, Dunnett's test; Figure 3C). This demonstrated that presynaptic DOR signaling in PV+ neurons does not require PKA and, instead, is likely mediated by Gβγ-mediated mechanisms.

If DORs suppress release by altering presynaptic $Ca_V$ function, then this should be evident by imaging Ca influx at terminals. To test this, mPFC slices were obtained from fluorescent reporter mice (PV-Ai14) that allowed identification of PV+ somata via two-photon microscopy. Whole-cell patch-clamp recordings were made from fluorescent cells in L5, and cells were loaded with the volume-filling dye Alexa Fluor 594 (20 µM) and the Ca indicator Fluo-5F (250 µM) (Figure 3D). PV+ interneuron identity was validated through neurophysiological characterization (low $R_{input}$, high-frequency AP firing with pronounced AP afterhyperpolarization [AHP]). A burst of 3 APs was then evoked, and the resultant AP-evoked Ca influx was imaged at boutons (Figure 3E). Robust Ca transients were elicited reliably by this protocol and stable over 40 min in control conditions. Following the application of DPDPE, AP-evoked Ca transients decreased significantly (Norm ΔG/R; vehicle vs. DPDPE = 0.90 ± 0.04 vs. 0.54 ± 0.03, $n/N$ = 6/3 vs. 6/3; $p$ = 0.00011; Figures 3F and 3G), demonstrating that DORs inhibit presynaptic $Ca_V$ in PV+ terminals. Additionally, DPDPE lowered $R_{input}$ (Figure S4B) and increased outward holding currents (Figure S4C) corresponding to membrane hyperpolarization, likely through GIRK activation.[37] These results demonstrate that DORs strongly inhibit PV+ output, influencing both somatodendritic and axonal compartments, and suppress release from PV+ terminals by modulating $Ca_V$s.

## DORs engage multiple modulatory cascades in SOM+ neurons

Excitatory synapses in mPFC express two forms of presynaptic modulation: a canonical $G_{i/o}$-Gβγ pathway (i.e., $GABA_BR$) and non-canonical signaling via $G_s$ and PKA (i.e., D1R).[35] DOR-dependent modulation in SOM+ terminals, by contrast, appears intermediate between these two mechanisms. Thus, we hypothesize that DORs engage two independent signaling cascades in SOM+ terminals that converge on $Ca_V$s. If true, then each signaling cascade should contribute partially to the total reduction in IPSC amplitude but with different effects on the PPR. These different effects could then sum to yield an intermediate PPR result that lies between canonical and gain modulation (Figure 2E).

Testing this requires selective block of the two putative signaling cascades driven by $G_{i/o}$-Gβγ and $G_s$-PKA. While PKA activity can be easily blocked in slice preparations, blockade of $G_{i/o}$-Gβγ is more difficult. Pertussis toxin (PTx)—a highly potent and specific inhibitor of $G_{i/o}$-coupled signaling—requires prolonged exposure (>24 h) to achieve a saturating effect in tissue,[52,53] making it unwieldy for traditional slice experiments. To achieve this saturating block, we delivered PTx via stereotaxic injection locally to mPFC, 1–3 days prior to slice preparation, in SOM-Cre mice previously infected with ChR2-expressing viruses (Figure 4A). This strategy was chosen over other delivery methods due to its increased efficacy (see STAR Methods, but see also Tang and Lovinger[49] and Thalmann[50]). To confirm that $G_{i/o}$-Gβγ signaling was attenuated by this method, we assayed $GABA_B$-dependent modulation of electrically evoked EPSCs with 1 µM baclofen in one slice from each animal. Baclofen reduced eEPSCs by 77% in uninjected slices ($n/N$ = 5/2, $p < 0.0001$), comparable to prior observations.[23,54] By contrast, baclofen reduced eEPSCs by only 10% in slices from PTx-treated animals (Norm EPSC: 0.90 ± 0.02, $n/N$ = 10/8;

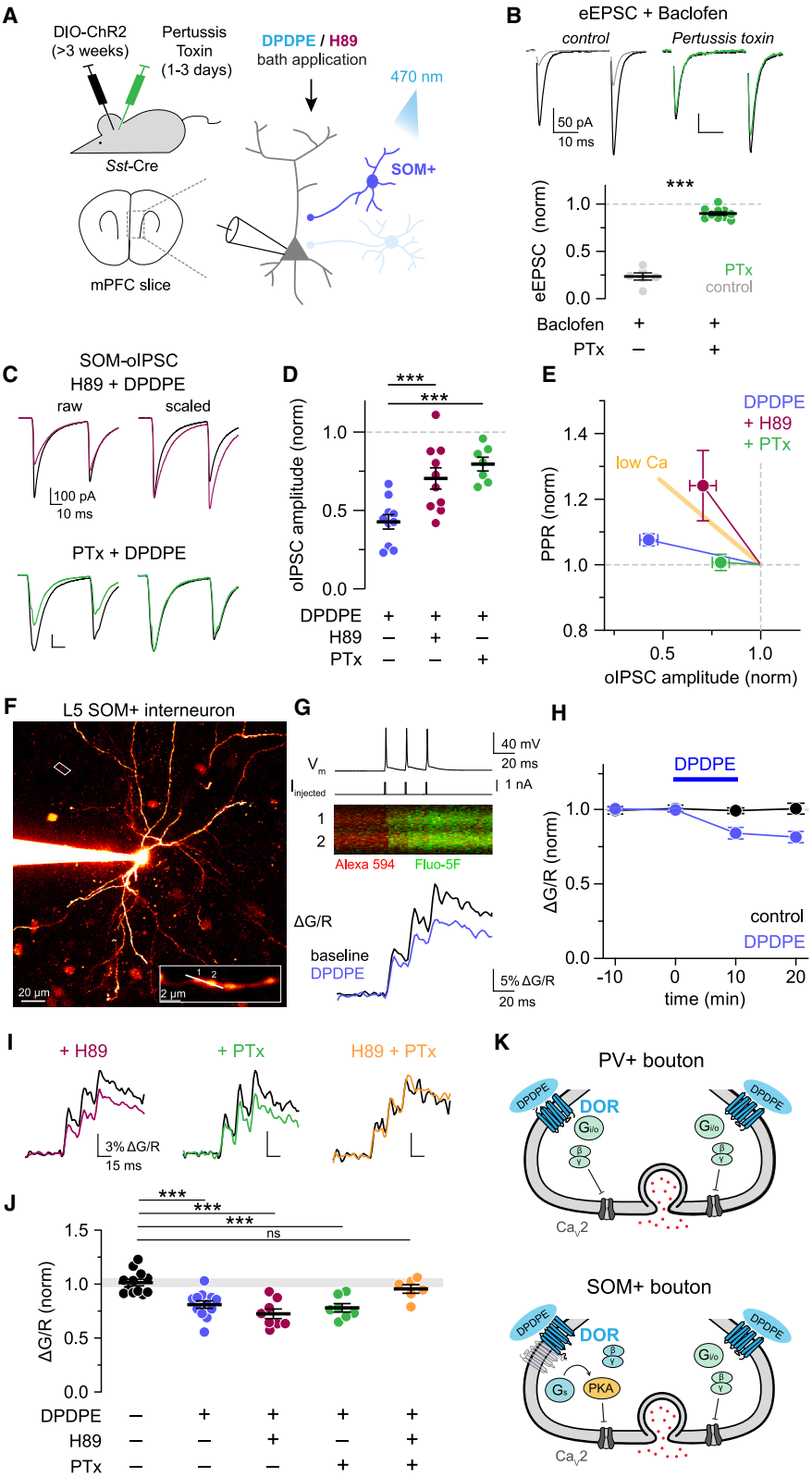


(legend on next page)

$p < 0.0001$; Figure 4B), indicating that the majority of $G_{i/o}$ signaling was blocked with this approach.

Following PTx validation, SOM-oIPSCs were evoked as described earlier (Figure 2). In these conditions, DPDPE application still reduced oIPSCs in PTx-injected slices (Norm oIPSC = 0.80 ± 0.04, $n/N$ = 7/3; $p = 0.0034$), though to a lesser degree compared to DPDPE application in the absence of PTx ($p = 0.0006$, Holm-Sidak post hoc test; Figures 4C and 4D). Similar effects were observed with the PKA blocker H89 ($p = 0.0025$, Holm-Sidak post hoc test). Strikingly, the amplitude-PPR relationships were completely distinct for PTx and H89 conditions. With PKA blocked, the residual modulation was completely canonical, overlaying with low Ca. With $G_{i/o}$-Gβγ blocked, the PPR was not altered (Figure 4E). Taken together, these results demonstrate that DORs regulate SOM+ GABA release through two mechanisms: one that is $G_{i/o}$ dependent that increases the PPR and another that is $G_{i/o}$ independent but PKA dependent that does not alter the PPR.

While the data above indicate that DORs engage two separate signaling cascades to regulate release from SOM+ terminals, because IPSCs are the aggregate of activity across multiple synapses, they cannot inform whether both cascades are engaged within single terminals or selectively on a terminal-by-terminal basis, perhaps based on the SOM+ cell subclass. SOM is expressed by a range of interneuron subclasses that can be grouped by intrinsic electrophysiological characteristics.[55–57] Indeed, when recording directly from SOM+ cells, we identified two distinct neurophysiological phenotypes, with some neurons exhibiting high $R_{input}$, slow $\tau_{membrane}$, and small AHPs and others with lower $R_{input}$, faster $\tau_{membrane}$, larger AHP, and quasi-fast-spiking behavior akin to PV+ neurons (Figure S5B). These two subgroups are defined as putative Martinotti (MC) and non-Martinotti (NMC) cells[58] and contrast with PV+ neurons further due to their repetitive spike patterns and AP waveforms (Figure S5D). We therefore made whole-cell recordings from each of these classes and imaged AP-evoked Ca influx in boutons (Figures 4F and 4G). The P/Q- and N-type $Ca_V$ inhibitor ω-conotoxin-MVIIC (1 μM) reduced AP-evoked Ca transients by 72.6% (Figures S6D and S6E), indicating that these isoforms mediate the majority of Ca entry in SOM+ terminals. Ca transients were reduced by DPDPE in all boutons imaged, independent of SOM subclass (Norm ΔG/R in MCs: vehicle vs. DPDPE = 1.00 ± 0.03 vs. 0.81 ± 0.03, $n/N$ = 11/9 vs. 12/8; $p = 0.0007$; NMCs: $p < 0.0001$, Holm-Sidak post hoc test; Figure 4H and S5E-G). Remarkably, DPDPE was similarly effective in all boutons imaged in the presence of H89 or PTx (H89: $p = 0.36$; PTx: $p = 0.66$, Holm-Sidak post hoc test; Figures 4I and 4J). The combined application of H89 and PTx completely eliminated the effect of DPDPE on Ca transients in all SOM+ boutons imaged ($p = 0.66$, Holm-Sidak post hoc test; Figures 4I and 4J). Finally, the presence of ω-conotoxin-MVIIC occluded further suppression of bouton Ca by DPDPE (Figures S6D and S6E), demonstrating that DORs act via P/Q- and N-type $Ca_V$s. Taken together, these results indicate that DORs engage two distinct DOR signaling pathways within all SOM+ boutons, independent of SOM subclass, and that both cascades converge on presynaptic $Ca_V$s.

## DISCUSSION

Presynaptic opioid receptors engage a variety of intracellular cascades throughout the brain. Although $G_{i/o}$ (and specifically $G_{i/o}$-Gβγ) signaling is common, other pathways mobilize β-arrestin or $G_q$ subunits that may regulate HCN or $K_V$ channels instead of $Ca_V$s and GIRK.[27,59] Pleiotropic signaling that regulates transmitter release via simultaneous, parallel pathways may be more common than previously appreciated. If opioid receptors regulate transmitter release by reducing $P_R$, then the PPR should consistently and proportionately increase during opioid-mediated suppression. This assumption does not always hold true. Multiple studies of opioid-dependent synaptic regulation suggest that modulation occurs presynaptically, even when the PPR changes only slightly or not at all.[31–34,60] While there are $Ca_V$-independent mechanisms that could account for some aspects of these effects,[61,62] we show here that parallel signaling cascades converging on $Ca_V$s can account for modulation entirely in these GABAergic terminals.

Revisiting prior findings through this lens suggests that this pleiotropic signaling may be engaged at multiple synapses by multiple opioid receptors. Studies often conclude that G-protein-coupled receptors (GPCRs) are acting presynaptically if *any* increase in the PPR is observed. But here, we show that the magnitude of PPR change, benchmarked against how much it should change via canonical mechanisms, can inform on *how*

**Figure 4. SOM+ interneurons exhibit heterogeneous regulation by DORs**

(A) Cartoon depicting injection schedule for electrophysiology experiments involving pertussis toxin (PTx).

(B) Top: example EPSC traces in L5 pyramidal neurons evoked by electrical stimulation before (black) and after (gray or green) application of baclofen in control mice (left) or those injected with PTx (right). Bottom: summary plot of normalized eEPSC amplitudes after baclofen application.

(C) Example SOM-oIPSC traces before and after DPDPE with either H89 pre-incubation (top) or injected PTx (bottom).

(D) Summary plot of normalized oIPSC amplitudes after DPDPE in control (blue), H89 (maroon), and PTx (green) conditions.

(E) Normalized amplitude-PPR plot depicting slope relationships for SOM-oIPSCs in all conditions.

(F) z stack image of filled SOM+ interneuron. Imaging location (white box) is enlarged and rotated in the inset (bottom left). The line-scan ROI is represented as a white bar.

(G) Top: raw APs evoked by step protocol. Middle: superimposed Alexa 594 (red) and Fluo-5F (green) signals from boutons in line-scan ROI. Bottom: example Ca transients from ΔG/R fluorescence data at baseline and after DPDPE application.

(H) Summary time course plot of normalized peak ΔG/R in SOM+ boutons for control and DPDPE conditions.

(I) Example AP-evoked Ca transients before and after DPDPE with H89, locally injected PTx, or both.

(J) Summary normalized peak ΔG/R data in control and drug conditions.

(K) Schematic depicting DOR-dependent signaling pathway in PV+ and SOM+ boutons.

Data are depicted as mean ± SEM. *** $p < 0.001$; ns, non-significant.

$Ca_V$s are being modulated. As a case in point, DORs at nucleus raphe magnus synapses reduce EPSC amplitude ~50%, while the PPR increases by only 12%,[63] a change far too small to be explained via canonical mechanisms. There are comparable observations found elsewhere,[37,38,64,65] where GPCRs cause substantial synaptic depression with only modest, yet statistically significant, effects on the PPR. That intermediate PPR change can result from the combination of multiple pathways has implications for interpreting presynaptic opioid effects more broadly and suggests that a new framework is necessary.

## $G_{i/o}$-independent opioid receptor signaling

How could $G_{i/o}$-coupled DORs signal via $G_s$?[66,67] One possibility is that DORs heterodimerize with $G_s$-coupled receptors in SOM+ terminals. Heterodimeric GPCR complexes consist of two different receptor protomers that oligomerize directly or via shared adenylyl cyclases (ACs).[68] DORs form heterodimers with both MORs and kappa opioid receptors (KORs),[69,70] as well as with cannabinoid and chemokine receptors,[71,72] affecting desensitization, pharmacological efficacy, and signaling bias. $G_s$ and $G_{i/o}$ receptors, though having opposed downstream effects, can also oligomerize in heterodimeric complexes. For example, $G_s$-coupled adenosine $A_{2A}$ and $G_{i/o}$-coupled dopamine D2 receptors form a common functional unit with AC5 proteins, each exerting allosteric control over the catalyzation of cAMP.[73] DORs have also been shown to co-immunoprecipitate with $G_s$-coupled β2 adrenergic receptors in cardiac tissue,[74] establishing physiological precedent for DOR-containing $G_s$-$G_{i/o}$ heterodimers.

GPCR heterodimers are attractive therapeutic targets, potentially offering tissue specificity and limited side effects compared to receptor protomers or homodimers.[68] Selective pharmacology has been developed for a small subset of discovered heterodimer pairs, including $mGluR_{2/4}$ receptors.[75] A combination of positive and negative allosteric modulators was used to show that mGluR heteromers, but not homomers, regulate thalamic inputs to mPFC but not those from hippocampus or amygdala.[76] Targeting peripheral MOR/DOR or MOR/KOR heterodimers has shown promise for producing analgesia with less tolerance and withdrawal effects, but the functional relevance of opioid receptor heterodimers in the brain is less well characterized.[77]

## Functional implications

Both PV+ and SOM+ neurons exhibit strong presynaptic regulation by DORs, which would have compartment-specific effects in individual pyramidal cells. Perisomatic-targeting PV+ neurons are important for establishing synchronous firing, particularly in the gamma range (30–80 Hz),[78] of pyramidal cell networks in the neocortex and hippocampus.[79] $G_{i/o}$-Gβγ-dependent DOR signaling at these synapses imposes a high-pass filter on GABA release; therefore, the strength of inhibitory drive onto perisomatic compartments will recover during longer and higher-frequency stimuli. Brief disinhibition via DORs could tune the oscillatory phase of pyramidal activity on shorter timescales, as very few PV+ APs can control spike timing,[80] while preventing runaway network excitation on longer timescales.[81] Comparatively, SOM+ neurons instead modulate local dendritic excitability. In L5 neurons, this may affect the generation and propagation of dendritic Ca spikes, which are important for integrating signals from multiple brain areas.[82] SOM-derived GABA has been shown to suppress dendritic spikes,[83] so local disinhibition by DORs may increase the likelihood of such events and promote associative plasticity.[84] Such disinhibition and expansion of plasticity associative timing windows has been observed for the D2 dopaminergic regulation of interneurons in prefrontal cortex.[85] DOR-based regulation could therefore selectively promote the associative plasticity of long-range synaptic inputs that converge on apical dendrites. Given that DOR-mediated disinhibition at SOM+ terminals is less affected by presynaptic firing frequency, plasticity could be facilitated even during periods of elevated circuit activity. New intersectional genetic tools (i.e., conditional DOR deletion in either PV+ or SOM+ neurons) will be required to fully elucidate the role of differential DOR disinhibition on pyramidal cell computation and prefrontal circuit processing.

## Limitations of the study

Though we provide evidence of $G_{i/o}$-independent gain modulation at a subset of SOM+ terminals, the specific biophysical mechanism of $Ca_V$ regulation is unknown. $Ca_V$ channels may be regulated by direct PKA phosphorylation or through downstream activation of additional signaling molecules, which can be revealed by further experiments. Likewise, efforts should be made in the future to determine whether DORs engage PKA through a heterodimer complex. If they do, it will be important to determine the identity of this putative $G_s$-coupled partner. Finally, we observed putative NMCs that were identified in SOM-Cre mice. Given that these neurons are presumably targeted in ChR2 experiments, the relative contribution of NMC-derived inhibitory synaptic input remains unclear.

## RESOURCE AVAILABILITY

### Lead contact

Further inquiries and requests should be directed to the lead contact, Kevin J. Bender (kevin.bender@ucsf.edu).

### Materials availability

No new materials were generated in this study.

### Data and code availability

- This paper analyzes existing, publicly available data, accessible at https://portal.brain-map.org/atlases-and-data/rnaseq/mouse-whole-cortex-and-hippocampus-smart-seq.
- This paper does not report original code.
- Any additional information required to reanalyze the data reported in this paper is available from the lead contact upon request.

## ACKNOWLEDGMENTS

We are grateful to members of the Bender lab for comments and feedback. We thank Dr. Selin Schamiloglu for assistance with imaging analysis, Dr. Guy Bouvier for SOM-Cre mice, Dr. Elyssa Margolis for discussions regarding DOR pharmacology, and Dr. Dorit Ron for discussions related to $G_s$-$G_{i/o}$ heterodimers. This work was supported by NIH grants MH112729 and AA027023 (K.J.B.).

## AUTHOR CONTRIBUTIONS

R.P.D.A. and K.J.B. conceived the project and designed the experiments. R.P.D.A. performed all experiments and data analysis. R.P.D.A. and K.J.B. wrote the manuscript.

## DECLARATION OF INTERESTS

K.J.B. is on the scientific advisory board (SAB) for Regel Tx and receives research support from Regel Tx and BioMarin Pharmaceutical for projects not related to this work.

## STAR★METHODS

Detailed methods are provided in the online version of this paper and include the following:

- KEY RESOURCES TABLE
- EXPERIMENTAL MODEL AND STUDY PARTICIPANT DETAILS
  - Mouse strains
- METHOD DETAILS
  - Stereotaxic injections
  - Slice preparation
  - *Ex vivo* electrophysiology
  - 2-Photon microscopy
- QUANTIFICATION AND STATISTICAL ANALYSIS

## SUPPLEMENTAL INFORMATION

Supplemental information can be found online at https://doi.org/10.1016/j.celrep.2025.115293.

Received: July 18, 2024
Revised: November 22, 2024
Accepted: January 20, 2025
Published: February 8, 2025

## REFERENCES

1. Mansour, A., Fox, C.A., Akil, H., and Watson, S.J. (1995). Opioid-receptor mRNA expression in the rat CNS: anatomical and functional implications. Trends Neurosci. *18*, 22–29. https://doi.org/10.1016/0166-2236(95)93946-u.
2. Waldhoer, M., Bartlett, S.E., and Whistler, J.L. (2004). Opioid receptors. Annu. Rev. Biochem. *73*, 953–990. https://doi.org/10.1146/annurev.biochem.73.011303.073940.
3. Le Merrer, J., Becker, J.A.J., Befort, K., and Kieffer, B.L. (2009). Reward processing by the opioid system in the brain. Physiol. Rev. *89*, 1379–1412. https://doi.org/10.1152/physrev.00005.2009.
4. Contet, C., Kieffer, B.L., and Befort, K. (2004). Mu opioid receptor: a gateway to drug addiction. Curr. Opin. Neurobiol. *14*, 370–378. https://doi.org/10.1016/j.conb.2004.05.005.
5. Kieffer, B.L., and Gavériaux-Ruff, C. (2002). Exploring the opioid system by gene knockout. Prog. Neurobiol. *66*, 285–306. https://doi.org/10.1016/s0301-0082(02)00008-4.
6. Chu Sin Chung, P., and Kieffer, B.L. (2013). Delta opioid receptors in brain function and diseases. Pharmacol. Ther. *140*, 112–120. https://doi.org/10.1016/j.pharmthera.2013.06.003.
7. Pradhan, A.A., Befort, K., Nozaki, C., Gavériaux-Ruff, C., and Kieffer, B.L. (2011). The delta opioid receptor: an evolving target for the treatment of brain disorders. Trends Pharmacol. Sci. *32*, 581–590. https://doi.org/10.1016/j.tips.2011.06.008.
8. Quirion, B., Bergeron, F., Blais, V., and Gendron, L. (2020). The Delta-Opioid Receptor; a Target for the Treatment of Pain. Front. Mol. Neurosci. *13*, 52. https://doi.org/10.3389/fnmol.2020.00052.
9. Margolis, E.B., Fields, H.L., Hjelmstad, G.O., and Mitchell, J.M. (2008). Delta-opioid receptor expression in the ventral tegmental area protects against elevated alcohol consumption. J. Neurosci. *28*, 12672–12681. https://doi.org/10.1523/JNEUROSCI.4569-08.2008.
10. Nielsen, C.K., Simms, J.A., Pierson, H.B., Li, R., Saini, S.K., Ananthan, S., and Bartlett, S.E. (2008). A novel delta opioid receptor antagonist, SoRI-9409, produces a selective and long-lasting decrease in ethanol consumption in heavy-drinking rats. Biol. Psychiatr. *64*, 974–981. https://doi.org/10.1016/j.biopsych.2008.07.018.
11. Chefer, V.I., and Shippenberg, T.S. (2009). Augmentation of morphine-induced sensitization but reduction in morphine tolerance and reward in delta-opioid receptor knockout mice. Neuropsychopharmacology *34*, 887–898. https://doi.org/10.1038/npp.2008.128.
12. Scherrer, G., Imamachi, N., Cao, Y.Q., Contet, C., Mennicken, F., O'Donnell, D., Kieffer, B.L., and Basbaum, A.I. (2009). Dissociation of the opioid receptor mechanisms that control mechanical and heat pain. Cell *137*, 1148–1159. https://doi.org/10.1016/j.cell.2009.04.019.
13. Chu Sin Chung, P., Keyworth, H.L., Martin-Garcia, E., Charbogne, P., Darcq, E., Bailey, A., Filliol, D., Matifas, A., Scherrer, G., Ouagazzal, A.M., et al. (2015). A novel anxiogenic role for the delta opioid receptor expressed in GABAergic forebrain neurons. Biol. Psychiatr. *77*, 404–415. https://doi.org/10.1016/j.biopsych.2014.07.033.
14. Chung, P.C.S., Boehrer, A., Stephan, A., Matifas, A., Scherrer, G., Darcq, E., Befort, K., and Kieffer, B.L. (2015). Delta opioid receptors expressed in forebrain GABAergic neurons are responsible for SNC80-induced seizures. Behav. Brain Res. *278*, 429–434. https://doi.org/10.1016/j.bbr.2014.10.029.
15. Saitoh, A., Suzuki, S., Soda, A., Ohashi, M., Yamada, M., Oka, J.I., Nagase, H., and Yamada, M. (2018). The delta opioid receptor agonist KNT-127 in the prelimbic medial prefrontal cortex attenuates veratrine-induced anxiety-like behaviors in mice. Behav. Brain Res. *336*, 77–84. https://doi.org/10.1016/j.bbr.2017.08.041.
16. Baldo, B.A. (2016). Prefrontal Cortical Opioids and Dysregulated Motivation: A Network Hypothesis. Trends Neurosci. *39*, 366–377. https://doi.org/10.1016/j.tins.2016.03.004.
17. Koob, G.F. (2020). Neurobiology of Opioid Addiction: Opponent Process, Hyperkatifeia, and Negative Reinforcement. Biol. Psychiatr. *87*, 44–53. https://doi.org/10.1016/j.biopsych.2019.05.023.
18. Jiang, C., Wang, X., Le, Q., Liu, P., Liu, C., Wang, Z., He, G., Zheng, P., Wang, F., and Ma, L. (2021). Morphine coordinates SST and PV interneurons in the prelimbic cortex to disinhibit pyramidal neurons and enhance reward. Mol. Psychiatr. *26*, 1178–1193. https://doi.org/10.1038/s41380-019-0480-7.
19. Olive, M.F., Anton, B., Micevych, P., Evans, C.J., and Maidment, N.T. (1997). Presynaptic versus postsynaptic localization of mu and delta opioid receptors in dorsal and ventral striatopallidal pathways. J. Neurosci. *17*, 7471–7479. https://doi.org/10.1523/JNEUROSCI.17-19-07471.1997.
20. Ostermeier, A.M., Schlösser, B., Schwender, D., and Sutor, B. (2000). Activation of mu- and delta-opioid receptors causes presynaptic inhibition of glutamatergic excitation in neocortical neurons. Anesthesiology *93*, 1053–1063. https://doi.org/10.1097/00000542-200010000-00029.
21. Che, T., and Roth, B.L. (2023). Molecular basis of opioid receptor signaling. Cell *186*, 5203–5219. https://doi.org/10.1016/j.cell.2023.10.029.
22. Morikawa, H., Mima, H., Uga, H., Shoda, T., and Fukuda, K. (1999). Opioid potentiation of N-type Ca2+ channel currents via pertussis-toxin-sensitive G proteins in NG108-15 cells. Pflügers Archiv *438*, 423–426. https://doi.org/10.1007/pl00008091.
23. Mintz, I.M., and Bean, B.P. (1993). GABAB receptor inhibition of P-type Ca2+ channels in central neurons. Neuron *10*, 889–898. https://doi.org/10.1016/0896-6273(93)90204-5.
24. Bean, B.P. (1989). Neurotransmitter inhibition of neuronal calcium currents by changes in channel voltage dependence. Nature *340*, 153–156. https://doi.org/10.1038/340153a0.
25. Herlitze, S., Garcia, D.E., Mackie, K., Hille, B., Scheuer, T., and Catterall, W.A. (1996). Modulation of Ca2+ channels by G-protein beta gamma subunits. Nature *380*, 258–262. https://doi.org/10.1038/380258a0.
26. Al-Hasani, R., and Bruchas, M.R. (2011). Molecular mechanisms of opioid receptor-dependent signaling and behavior. Anesthesiology *115*, 1363–1381. https://doi.org/10.1097/ALN.0b013e318238bba6.

27. Reeves, K.C., Shah, N., Muñoz, B., and Atwood, B.K. (2022). Opioid Receptor-Mediated Regulation of Neurotransmission in the Brain. Front. Mol. Neurosci. *15*, 919773. https://doi.org/10.3389/fnmol.2022.919773.

28. Atwood, B.K., Lovinger, D.M., and Mathur, B.N. (2014). Presynaptic long-term depression mediated by Gi/o-coupled receptors. Trends Neurosci. *37*, 663–673. https://doi.org/10.1016/j.tins.2014.07.010.

29. Lovinger, D.M., Mateo, Y., Johnson, K.A., Engi, S.A., Antonazzo, M., and Cheer, J.F. (2022). Local modulation by presynaptic receptors controls neuronal communication and behaviour. Nat. Rev. Neurosci. *23*, 191–203. https://doi.org/10.1038/s41583-022-00561-0.

30. Jackman, S.L., and Regehr, W.G. (2017). The Mechanisms and Functions of Synaptic Facilitation. Neuron *94*, 447–464. https://doi.org/10.1016/j.neuron.2017.02.047.

31. Lau, B.K., Ambrose, B.P., Thomas, C.S., Qiao, M., and Borgland, S.L. (2020). Mu-Opioids Suppress GABAergic Synaptic Transmission onto Orbitofrontal Cortex Pyramidal Neurons with Subregional Selectivity. J. Neurosci. *40*, 5894–5907. https://doi.org/10.1523/JNEUROSCI.2049-19.2020.

32. Li, C., Pleil, K.E., Stamatakis, A.M., Busan, S., Vong, L., Lowell, B.B., Stuber, G.D., and Kash, T.L. (2012). Presynaptic inhibition of gamma-aminobutyric acid release in the bed nucleus of the stria terminalis by kappa opioid receptor signaling. Biol. Psychiatr. *71*, 725–732. https://doi.org/10.1016/j.biopsych.2011.11.015.

33. Tejeda, H.A., Wu, J., Kornspun, A.R., Pignatelli, M., Kashtelyan, V., Krashes, M.J., Lowell, B.B., Carlezon, W.A., Jr., and Bonci, A. (2017). Pathway- and Cell-Specific Kappa-Opioid Receptor Modulation of Excitation-Inhibition Balance Differentially Gates D1 and D2 Accumbens Neuron Activity. Neuron *93*, 147–163. https://doi.org/10.1016/j.neuron.2016.12.005.

34. Yokota, E., Koyanagi, Y., Yamamoto, K., Oi, Y., Koshikawa, N., and Kobayashi, M. (2016). Opioid subtype- and cell-type-dependent regulation of inhibitory synaptic transmission in the rat insular cortex. Neuroscience *339*, 478–490. https://doi.org/10.1016/j.neuroscience.2016.10.004.

35. Burke, K.J., Jr., Keeshen, C.M., and Bender, K.J. (2018). Two Forms of Synaptic Depression Produced by Differential Neuromodulation of Presynaptic Calcium Channels. Neuron *99*, 969–984. https://doi.org/10.1016/j.neuron.2018.07.030.

36. van Rijn, R.M., Defriel, J.N., and Whistler, J.L. (2013). Pharmacological traits of delta opioid receptors: pitfalls or opportunities? Psychopharmacology (Berl) *228*, 1–18. https://doi.org/10.1007/s00213-013-3129-2.

37. He, X.J., Patel, J., Weiss, C.E., Ma, X., Bloodgood, B.L., and Banghart, M.R. (2021). Convergent, functionally independent signaling by mu and delta opioid receptors in hippocampal parvalbumin interneurons. Elife *10*, e69746. https://doi.org/10.7554/eLife.69746.

38. Shen, K.Z., and Johnson, S.W. (2002). Presynaptic modulation of synaptic transmission by opioid receptor in rat subthalamic nucleus in vitro. J. Physiol. *541*, 219–230. https://doi.org/10.1113/jphysiol.2001.013404.

39. Yamada, D., Takahashi, J., Iio, K., Nagase, H., and Saitoh, A. (2021). Modulation of glutamatergic synaptic transmission and neuronal excitability in the prelimbic medial prefrontal cortex via delta-opioid receptors in mice. Biochem. Biophys. Res. Commun. *560*, 192–198. https://doi.org/10.1016/j.bbrc.2021.05.002.

40. Brenowitz, S., David, J., and Trussell, L. (1998). Enhancement of synaptic efficacy by presynaptic GABA(B) receptors. Neuron *20*, 135–141. https://doi.org/10.1016/s0896-6273(00)80441-9.

41. Kruglikov, I., and Rudy, B. (2008). Perisomatic GABA release and thalamocortical integration onto neocortical excitatory cells are regulated by neuromodulators. Neuron *58*, 911–924. https://doi.org/10.1016/j.neuron.2008.04.024.

42. Hjelmstad, G.O., and Fields, H.L. (2001). Kappa opioid receptor inhibition of glutamatergic transmission in the nucleus accumbens shell. J. Neurophysiol. *85*, 1153–1158. https://doi.org/10.1152/jn.2001.85.3.1153.

43. Yao, Z., van Velthoven, C.T.J., Nguyen, T.N., Goldy, J., Sedeno-Cortes, A.E., Baftizadeh, F., Bertagnolli, D., Casper, T., Chiang, M., Crichton, K., et al. (2021). A taxonomy of transcriptomic cell types across the isocortex and hippocampal formation. Cell *184*, 3222–3241. https://doi.org/10.1016/j.cell.2021.04.021.

44. Lim, L., Mi, D., Llorca, A., and Marín, O. (2018). Development and Functional Diversification of Cortical Interneurons. Neuron *100*, 294–313. https://doi.org/10.1016/j.neuron.2018.10.009.

45. Bucurenciu, I., Kulik, A., Schwaller, B., Frotscher, M., and Jonas, P. (2008). Nanodomain coupling between Ca2+ channels and Ca2+ sensors promotes fast and efficient transmitter release at a cortical GABAergic synapse. Neuron *57*, 536–545. https://doi.org/10.1016/j.neuron.2007.12.026.

46. Eggermann, E., and Jonas, P. (2011). How the 'slow' Ca(2+) buffer parvalbumin affects transmitter release in nanodomain-coupling regimes. Nat. Neurosci. *15*, 20–22. https://doi.org/10.1038/nn.3002.

47. Scimemi, A., and Diamond, J.S. (2012). The number and organization of Ca2+ channels in the active zone shapes neurotransmitter release from Schaffer collateral synapses. J. Neurosci. *32*, 18157–18176. https://doi.org/10.1523/JNEUROSCI.3827-12.2012.

48. Jordan, B., and Devi, L.A. (1998). Molecular mechanisms of opioid receptor signal transduction. Br. J. Anaesth. *81*, 12–19. https://doi.org/10.1093/bja/81.1.12.

49. Tang, K.C., and Lovinger, D.M. (2000). Role of pertussis toxin-sensitive G-proteins in synaptic transmission and plasticity at corticostriatal synapses. J. Neurophysiol. *83*, 60–69. https://doi.org/10.1152/jn.2000.83.1.60.

50. Thalmann, R.H. (1988). Evidence that guanosine triphosphate (GTP)-binding proteins control a synaptic response in brain: effect of pertussis toxin and GTP gamma S on the late inhibitory postsynaptic potential of hippocampal CA3 neurons. J. Neurosci. *8*, 4589–4602. https://doi.org/10.1523/JNEUROSCI.08-12-04589.1988.

51. Ikeda, S.R. (1996). Voltage-dependent modulation of N-type calcium channels by G-protein beta gamma subunits. Nature *380*, 255–258. https://doi.org/10.1038/380255a0.

52. Aghajanian, G.K., and Wang, Y.Y. (1986). Pertussis toxin blocks the outward currents evoked by opiate and alpha 2-agonists in locus coeruleus neurons. Brain Res. *371*, 390–394. https://doi.org/10.1016/0006-8993(86)90382-3.

53. Inoue, M., Nakajima, S., and Nakajima, Y. (1988). Somatostatin induces an inward rectification in rat locus coeruleus neurones through a pertussis toxin-sensitive mechanism. J. Physiol. *407*, 177–198. https://doi.org/10.1113/jphysiol.1988.sp017409.

54. Tatebayashi, H., and Ogata, N. (1992). GABAB-mediated modulation of the voltage-gated Ca2+ channels. Gen. Pharmacol. *23*, 309–316. https://doi.org/10.1016/0306-3623(92)90088-2.

55. Ma, Y., Hu, H., Berrebi, A.S., Mathers, P.H., and Agmon, A. (2006). Distinct subtypes of somatostatin-containing neocortical interneurons revealed in transgenic mice. J. Neurosci. *26*, 5069–5082. https://doi.org/10.1523/JNEUROSCI.0661-06.2006.

56. Naka, A., Veit, J., Shababo, B., Chance, R.K., Risso, D., Stafford, D., Snyder, B., Egladyous, A., Chu, D., Sridharan, S., et al. (2019). Complementary networks of cortical somatostatin interneurons enforce layer specific control. Elife *8*, 43696. https://doi.org/10.7554/eLife.43696.

57. Wu, S.J., Sevier, E., Dwivedi, D., Saldi, G.A., Hairston, A., Yu, S., Abbott, L., Choi, D.H., Sherer, M., Qiu, Y., et al. (2023). Cortical somatostatin interneuron subtypes form cell-type-specific circuits. Neuron *111*, 2675–2692. https://doi.org/10.1016/j.neuron.2023.05.032.

58. Riedemann, T. (2019). Diversity and Function of Somatostatin-Expressing Interneurons in the Cerebral Cortex. Int. J. Mol. Sci. *20*, 2952. https://doi.org/10.3390/ijms20122952.

59. Coutens, B., and Ingram, S.L. (2023). Key differences in regulation of opioid receptors localized to presynaptic terminals compared to somas: Relevance for novel therapeutics. Neuropharmacology *226*, 109408. https://doi.org/10.1016/j.neuropharm.2022.109408.

60. Banghart, M.R., Neufeld, S.Q., Wong, N.C., and Sabatini, B.L. (2015). Enkephalin Disinhibits Mu Opioid Receptor-Rich Striatal Patches via Delta Opioid Receptors. Neuron *88*, 1227–1239. https://doi.org/10.1016/j.neuron.2015.11.010.

61. Blackmer, T., Larsen, E.C., Takahashi, M., Martin, T.F., Alford, S., and Hamm, H.E. (2001). G protein betagamma subunit-mediated presynaptic inhibition: regulation of exocytotic fusion downstream of Ca2+ entry. Science *292*, 293–297. https://doi.org/10.1126/science.1058803.

62. Capogna, M., Gahwiler, B.H., and Thompson, S.M. (1993). Mechanism of mu-opioid receptor-mediated presynaptic inhibition in the rat hippocampus in vitro. J. Physiol. *470*, 539–558. https://doi.org/10.1113/jphysiol.1993.sp019874.

63. Zhang, Z., and Pan, Z.Z. (2010). Synaptic mechanism for functional synergism between delta- and mu-opioid receptors. J. Neurosci. *30*, 4735–4745. https://doi.org/10.1523/JNEUROSCI.5968-09.2010.

64. Edwards, J.G., Gibson, H.E., Jensen, T., Nugent, F., Walther, C., Blickenstaff, J., and Kauer, J.A. (2012). A novel non-CB1/TRPV1 endocannabinoid-mediated mechanism depresses excitatory synapses on hippocampal CA1 interneurons. Hippocampus *22*, 209–221. https://doi.org/10.1002/hipo.20884.

65. Winters, B.L., Gregoriou, G.C., Kissiwaa, S.A., Wells, O.A., Medagoda, D.I., Hermes, S.M., Burford, N.T., Alt, A., Aicher, S.A., and Bagley, E.E. (2017). Endogenous opioids regulate moment-to-moment neuronal communication and excitability. Nat. Commun. *8*, 14611. https://doi.org/10.1038/ncomms14611.

66. Cruciani, R.A., Dvorkin, B., Morris, S.A., Crain, S.M., and Makman, M.H. (1993). Direct coupling of opioid receptors to both stimulatory and inhibitory guanine nucleotide-binding proteins in F-11 neuroblastoma-sensory neuron hybrid cells. Proc. Natl. Acad. Sci. USA *90*, 3019–3023. https://doi.org/10.1073/pnas.90.7.3019.

67. Fan, S.F., Shen, K.F., and Crain, S.M. (1991). Opioids at low concentration decrease openings of K+ channels in sensory ganglion neurons. Brain Res. *558*, 166–170. https://doi.org/10.1016/0006-8993(91)90737-g.

68. Ferre, S., Ciruela, F., Dessauer, C.W., Gonzalez-Maeso, J., Hebert, T.E., Jockers, R., Logothetis, D.E., and Pardo, L. (2022). G protein-coupled receptor-effector macromolecular membrane assemblies (GEMMAs). Pharmacol. Ther. *231*, 107977. https://doi.org/10.1016/j.pharmthera.2021.107977.

69. George, S.R., Fan, T., Xie, Z., Tse, R., Tam, V., Varghese, G., and O'Dowd, B.F. (2000). Oligomerization of mu- and delta-opioid receptors. Generation of novel functional properties. J. Biol. Chem. *275*, 26128–26135. https://doi.org/10.1074/jbc.M000345200.

70. Waldhoer, M., Fong, J., Jones, R.M., Lunzer, M.M., Sharma, S.K., Kostenis, E., Portoghese, P.S., and Whistler, J.L. (2005). A heterodimer-selective agonist shows in vivo relevance of G protein-coupled receptor dimers. Proc. Natl. Acad. Sci. USA *102*, 9050–9055. https://doi.org/10.1073/pnas.0501112102.

71. Rozenfeld, R., Bushlin, I., Gomes, I., Tzavaras, N., Gupta, A., Neves, S., Battini, L., Gusella, G.L., Lachmann, A., Ma'ayan, A., et al. (2012). Receptor heteromerization expands the repertoire of cannabinoid signaling in rodent neurons. PLoS One *7*, e29239. https://doi.org/10.1371/journal.pone.0029239.

72. Salanga, C.L., O'Hayre, M., and Handel, T. (2009). Modulation of chemokine receptor activity through dimerization and crosstalk. Cell. Mol. Life Sci. *66*, 1370–1386. https://doi.org/10.1007/s00018-008-8666-1.

73. Navarro, G., Cordomí, A., Casadó-Anguera, V., Moreno, E., Cai, N.S., Cortés, A., Canela, E.I., Dessauer, C.W., Casadó, V., Pardo, L., et al. (2018). Evidence for functional pre-coupled complexes of receptor heteromers and adenylyl cyclase. Nat. Commun. *9*, 1242. https://doi.org/10.1038/s41467-018-03522-3.

74. McVey, M., Ramsay, D., Kellett, E., Rees, S., Wilson, S., Pope, A.J., and Milligan, G. (2001). Monitoring receptor oligomerization using time-resolved fluorescence resonance energy transfer and bioluminescence resonance energy transfer. The human delta -opioid receptor displays constitutive oligomerization at the cell surface, which is not regulated by receptor occupancy. J. Biol. Chem. *276*, 14092–14099. https://doi.org/10.1074/jbc.M008902200.

75. Moreno Delgado, D., Moller, T.C., Ster, J., Giraldo, J., Maurel, D., Rovira, X., Scholler, P., Zwier, J.M., Perroy, J., Durroux, T., et al. (2017). Pharmacological evidence for a metabotropic glutamate receptor heterodimer in neuronal cells. Elife *6*, 25233. https://doi.org/10.7554/eLife.25233.

76. Xiang, Z., Lv, X., Lin, X., O'Brien, D.E., Altman, M.K., Lindsley, C.W., Javitch, J.A., Niswender, C.M., and Conn, P.J. (2021). Input-specific regulation of glutamatergic synaptic transmission in the medial prefrontal cortex by mGlu(2)/mGlu(4) receptor heterodimers. Sci. Signal. *14*, eabd2319. https://doi.org/10.1126/scisignal.abd2319.

77. Zhang, L., Zhang, J.T., Hang, L., and Liu, T. (2020). Mu Opioid Receptor Heterodimers Emerge as Novel Therapeutic Targets: Recent Progress and Future Perspective. Front. Pharmacol. *11*, 1078. https://doi.org/10.3389/fphar.2020.01078.

78. Gonzalez-Burgos, G., Cho, R.Y., and Lewis, D.A. (2015). Alterations in cortical network oscillations and parvalbumin neurons in schizophrenia. Biol. Psychiatr. *77*, 1031–1040. https://doi.org/10.1016/j.biopsych.2015.03.010.

79. Lewis, D.A. (2011). The chandelier neuron in schizophrenia. Dev. Neurobiol. *71*, 118–127. https://doi.org/10.1002/dneu.20825.

80. Veres, J.M., Nagy, G.A., Vereczki, V.K., Andrási, T., and Hájos, N. (2014). Strategically positioned inhibitory synapses of axo-axonic cells potently control principal neuron spiking in the basolateral amygdala. J. Neurosci. *34*, 16194–16206. https://doi.org/10.1523/JNEUROSCI.2232-14.2014.

81. Zhu, Y., Stornetta, R.L., and Zhu, J.J. (2004). Chandelier cells control excessive cortical excitation: characteristics of whisker-evoked synaptic responses of layer 2/3 nonpyramidal and pyramidal neurons. J. Neurosci. *24*, 5101–5108. https://doi.org/10.1523/JNEUROSCI.0544-04.2004.

82. Larkum, M.E., Wu, J., Duverdin, S.A., and Gidon, A. (2022). The Guide to Dendritic Spikes of the Mammalian Cortex In Vitro and In Vivo. Neuroscience *489*, 15–33. https://doi.org/10.1016/j.neuroscience.2022.02.009.

83. Palmer, L.M., Schulz, J.M., Murphy, S.C., Ledergerber, D., Murayama, M., and Larkum, M.E. (2012). The cellular basis of GABA(B)-mediated interhemispheric inhibition. Science *335*, 989–993. https://doi.org/10.1126/science.1217276.

84. Cichon, J., and Gan, W.B. (2015). Branch-specific dendritic Ca(2+) spikes cause persistent synaptic plasticity. Nature *520*, 180–185. https://doi.org/10.1038/nature14251.

85. Xu, T.X., and Yao, W.D. (2010). D1 and D2 dopamine receptors in separate circuits cooperate to drive associative long-term potentiation in the prefrontal cortex. Proc. Natl. Acad. Sci. USA *107*, 16366–16371. https://doi.org/10.1073/pnas.1004108107.

86. Alexander, R.P.D., Mitry, J., Sareen, V., Khadra, A., and Bowie, D. (2019). Cerebellar Stellate Cell Excitability Is Coordinated by Shifts in the Gating Behavior of Voltage-Gated Na(+) and A-Type K(+) Channels. eNeuro *6*, 0126-19.2019. https://doi.org/10.1523/ENEURO.0126-19.2019.

87. Tang, Z., Li, S., Han, P., Yin, J., Gan, Y., Liu, Q., Wang, J., Wang, C., Li, Y., and Shi, J. (2015). Pertussis toxin reduces calcium influx to protect ischemic stroke in a middle cerebral artery occlusion model. J. Neurochem. *135*, 998–1006. https://doi.org/10.1111/jnc.13359.

88. Chamberland, S., Nebet, E.R., Valero, M., Hanani, M., Egger, R., Larsen, S.B., Eyring, K.W., Buzsáki, G., and Tsien, R.W. (2023). Brief synaptic inhibition persistently interrupts firing of fast-spiking interneurons. Neuron *111*, 1264–1281. https://doi.org/10.1016/j.neuron.2023.01.017.

89. Bender, K.J., and Trussell, L.O. (2009). Axon initial segment Ca2+ channels influence action potential generation and timing. Neuron *61*, 259–271. https://doi.org/10.1016/j.neuron.2008.12.004.

## STAR★METHODS

### KEY RESOURCES TABLE

| REAGENT or RESOURCE | SOURCE | IDENTIFIER |
|---|---|---|
| Bacterial and virus strain | | |
| AAV5-Ef1α-DIO-hChR2(H134R)-eYFP | UNC Viral Core | N/A |
| Chemical, peptides, and recombinant proteins | | |
| DNQX disodium salt | Tocris | 2312 |
| DPDPE | Tocris | 1431 |
| [D-Ala2]-Deltorphin II | Tocris | 1180 |
| Naltrindole | Tocris | 0740 |
| SR 95531 hydrobromide | Tocris | 1262 |
| Pertussis toxin | Tocris | 3097 |
| (R)-Baclofen | Tocris | 0796 |
| H-89 dihydrochloride | Tocris | 2910 |
| Fluo-5F, Pentapotassium Salt, cell impermeant | Invitrogen | F14221 |
| Alexa Fluor 594 hydrazide | Invitrogen | A10438 |
| ω-conotoxin-MVIIC | Alomone | C-150 |
| Experimental models | | |
| Mouse: C57BL/6J | The Jackson Laboratory | RRID:IMSR_JAX:000664 |
| Mouse: B6; 129S6-Gt(ROSA)26Sor$^{tm14(CAG-tdTomato)Hze}$/J | The Jackson Laboratory | RRID:IMSR_JAX:007908 |
| Mouse: B6.129P2-Pvalb$^{tm1(cre)Arbr}$/J | The Jackson Laboratory | RRID:IMSR_JAX:017320 |
| Mouse: B6J.Cg-Sst$^{tm2.1(cre)Zjh}$/MwarJ | The Jackson Laboratory | RRID:IMSR_JAX:028864 |
| Deposited data | | |
| Cortex and hippocampus SMART-seq (mouse) | Yao et al.[43] | Allen Brain Map: https://portal.brain-map.org/atlases-and-data/rnaseq/mouse-whole-cortex-and-hippocampus-smart-seq |
| Software and algorithms | | |
| IGOR Pro | Wavemetrics | RRID: SCR_000325 |
| pClamp | Molecular Devices | RRID:SCR_011323 |
| Prism | GraphPad | RRID: SCR_002798 |
| MATLAB | Mathworks | RRID: SCR_001622 |
| FIJI | https://fiji.sc/ | RRID: SCR_002285 |

### EXPERIMENTAL MODEL AND STUDY PARTICIPANT DETAILS

#### Mouse strains

All procedures were performed in accordance with guidelines approved by the UCSF Institutional Animal Care and Use Committee (IACUC). All procedures conform to the relevant regulatory standards outlined by this committee. All experiments were performed on mice housed under a 12:12 h light/dark cycle with *ad libitum* access to food and water. C57BL/6J wild-type (JAX: 000664), C57PV-Cre$^{+/-}$ (JAX: 017320) and C57SOM-Cre$^{+/-}$ (JAX: 028864) mice were used for synaptic stimulation experiments. PV-Cre$^{+/-}$:Ai14 and SOM-Cre$^{+/-}$:Ai14 mice were used for 2-photon imaging experiments in cortical interneurons. Male and female mice aged postnatal day (P) 30–90 were used for all experiments. No significant differences based on sex were observed, and data were pooled between sexes.

### METHOD DETAILS

#### Stereotaxic injections

Subjects were injected with virus at P30-45. Prior to viral injection, mice were anesthetized by isofluorane and head-fixed in a stereotaxic frame. For channelrhodopsin stimulation experiments, subjects were then unilaterally injected with 400–600 nL of AAV5-EF1α-DIO-hChR2(H134R)-eYFP (''DIO-ChR2'') virus into left prefrontal cortex (from bregma: A/P +1.70, M/L −0.35, D/V

−2.60 mm). Acute slices were prepared approximately 4–6 weeks after injection. For PTx experiments, fresh lyophilized pertussis toxin powder (50 μg, Tocris) was obtained and reconstituted in PBS to 0.5 μg/μL and stored at 4°C (maximum 3 weeks). 2–2.5 μL PTx solution was injected into left PFC (same coordinates as above) at a rate of 150 nL/min. Following injection, the stereotaxic needle was left in place for 15 min before removing. Mice were used 24–72 h after surgery for electrophysiology experiments.

### Slice preparation

All experiments were performed in accordance with guidelines set by the University of California Animal Care and Use Committee. Mice aged P30-90 were anesthetized under isoflurane. Brains were dissected and placed in 4°C cutting solution consisting of (in mM): 87 NaCl, 25 $NaHCO_3$, 25 glucose, 75 sucrose, 2.5 KCl, 1.25 $NaH_2PO_4$, 0.5 $CaCl_2$, and 7 $MgCl_2$ and bubbled with 5% $CO_2$/95% $O_2$. 250 μm-thick coronal slices that included the medial prefrontal cortex were obtained via vibrating blade microtome (VT1200S, Leica). Slices were then incubated for 30 min at 33°C in a holding chamber with artificial cerebrospinal fluid (ACSF; see below). Following 30-min incubation, slices in holding chamber were placed at room temperature until recording, up to 8 h. All recordings were performed in ACSF at 32°C–34°C.

### *Ex vivo* electrophysiology

Slices were placed in recording chamber with circulating ACSF perfusion containing (in mM): 125 NaCl, 2.5 KCl, 1 $MgCl_2$, 25 $NaHCO_3$, 1.25 $NaH_2PO_4$, 25 glucose, bubbled with 5% $CO_2$/95% $O_2$, osmolarity adjusted to ∼300 mOsm. Before recording, ACSF was supplemented with 1.3 mM $CaCl_2$ from stock solution (except for 0.65 mM Ca experiments). Neurons were identified using differential interference contrast (DIC) optics for conventional visually-guided whole-cell recording, or with 2-photon-guided imaging of tdTomato fluorescence overlaid on a scanning DIC image of the slice. Patch electrodes were pulled from Schott 8250 glass (3–4 MΩ tip resistance). For voltage-clamp IPSC recordings, patch electrodes were filled with an internal solution that contained (in mM): 80 KCl, 40 $CsMeSO_4$, 10 HEPES, 4 NaCl, 5 QX-314, 10 $Na_2$-phosphocreatine, 4 Mg-ATP, 0.4 $Na_2$-GTP; 290 mOsm, pH 7.2–7.25. For current-clamp and voltage-clamp EPSC recordings, internal solution contained (in mM): 113 K-Gluconate, 9 HEPES, 4.5 $MgCl_2$, 14 $Tris_2$-phosphocreatine, 4 $Na_2$-ATP, 0.3 Tris-GTP; 290 mOsm, pH 7.2–7.25. Each recording day (if not imaging), internal solution was supplemented with 0.1 mM EGTA from stock.

Electrophysiological recordings were collected with a Multiclamp 700B amplifier (Molecular Devices) and a custom data acquisition program in Igor Pro software (Wavemetrics). Voltage-clamp recordings of synaptic currents were acquired at 20 kHz and filtered at 3 kHz. Current-clamp recordings were acquired at 20–50 kHz and filtered at 3–20 kHz. Whole-cell compensation of pipette capacitance (90%) and series resistance ($R_s$; 50%) were applied upon patch breakthrough. All data were corrected for measured junction potentials of +8 and +12 in high $Cl^-$ and K-gluconate-based internals, respectively. All recordings were made using a quartz electrode holder to minimize electrode drift within the slice. Data inclusion was based on the following criteria: $R_s$ <16 MΩ at baseline and <15% change over recording; holding leak current <-150 pA and <50 pA change; temperature change <1.5°C; $R_{input}$ <20% change. AP properties were measured in the first AP elicited by the current step after rheobase (rheobase+1). AP threshold was defined as the membrane potential when dV/dt first crossed 15 V/s. AHP amplitude was defined as the minimum voltage between APs relative to AP threshold. Membrane time constant ($\tau_{membrane}$) was determined by fitting an exponential to the hyperpolarization induced by a −50 pA step. $R_{input}$ was determined by −5 mV step in voltage-clamp (pyramidal), or multiple hyperpolarizing steps in current-clamp and taking the slope of the I-V relationship (interneurons). For examination of AP properties in L5 interneurons after Cd and Mn application, short current steps (15–40 ms; 20–160 pA) were applied every 10 s so that 1 AP was initiated reliably each sweep. Due to AP changes observed in the first 10 min (particularly in PV + neurons[86]), baseline (i.e., pre-drug) measurements were obtained >10 min following patch breakthrough. Divalent or time-locked control measurements were obtained 8–12 min after baseline/drug application.

Extracellular afferent stimulation was applied through a bipolar silver electrode in theta glass pipette connected to a battery. Patched neurons were held at −76 mV throughout recording. Pairs of stimuli were elicited through a pulse generator (0.2–0.8 V amplitude, 200 μs duration, 20 Hz frequency) at 15 s intervals to avoid induction of synaptic plasticity. The extracellular stimulating pipette was embedded in layer 5 neuropil ∼100–150 μm lateral from the recorded neuron to avoid direct stimulation. Optical stimulation of ChR2-expressing afferents was made via pairs of blue light flashes (472 nm LED, 0.5–2 $mW/mm^2$, 0.1–2 ms duration, 20 Hz frequency) through the 40X objective while whole-cell recording. To avoid polysynaptic responses, voltage amplitude/LED power were tuned so that responses were synchronous and monosynaptic, no failures were observed, and E/IPSC variability between sweeps was minimized. If necessary, the stimulating electrode or LED field-of-view would be moved to recruit more stable inputs.

For PTx experiments, mPFC slices from mice locally-injected with PTx were obtained as normal. Slices near the injection site were chosen for recording. Saturating PTx effect was verified in the first slice of each recording day by bath-applying 1 μM baclofen while measuring electrically-evoked EPSCs in L5 pyramidal neurons. If EPSC amplitude changed by more than 15%, the injection was considered a failure and no slices from that animal were used for DOR experiments. Previous attempts to achieve saturating PTx concentration in PFC included intraperitoneal[87] and intracerebroventricular[88] injection of PBS-PTx solution, where 1–1.5 μg total PTx was administered to each animal. Although significant differences were observed compared to control, the effect of baclofen was reduced by a maximum of ∼20%. Sufficient block (∼90%) of $G_{i/o}$ signaling was only achieved through local PTx injection.

### 2-Photon microscopy

For imaging experiments, a modified K-Gluconate-based internal was used where EGTA was replaced with 250 μM Fluo-5F and 20 μM Alexa 594 (Invitrogen). 2-photon laser scanning microscopy was performed as previously described.[89] A Coherent Ultra II was tuned to 810 nm for Ca imaging and morphology experiments. Fluorescence signals were captured either through a 40X, 0.8 NA objective for morphological imaging or a 60X, 1.0 NA objective for bouton Ca imaging paired with a 1.4 NA oil immersion condenser (Olympus). For Ca imaging, fluorescence was split into red and green channels using dichroic mirrors and band-pass filters (575 DCXR, ET525/70 m-2p, ET620/60 m-2p, Chroma). Green fluorescence (Fluo-5F) was captured with 10770-40 photomultiplier tubes (PMTs) selected for high quantum efficiency and low dark counts (Hamamatsu). Red fluorescence (Alexa 594) was captured with R9110 PMTs.

During bouton imaging, PV + or SOM+ neurons were first identified using tdTomato signal overlaid on DIC scanning of PV- or SOM-Ai14 reporter mice, respectively. Neurons were then patched and neurophysiological characterization was performed with cells held near −80 mV. Boutons were identified by imaging Alexa 594 in the red channel only and searching for thin processes relatively close to the slice surface exhibiting the characteristic string-of-pearls appearance (see Figures 3E and 4F). Ca imaging was initiated >15 min following patch breakthrough to allow sufficient dialysis and equilibration of both Alexa and Fluo dyes in distant axonal processes. Pairs of boutons were chosen if they were in the same z-plane and could be imaged simultaneously. This allowed us to detect instances of propagation failure and also compare modulation between neighboring boutons (Figure S7D and S7E). Trains of 3 APs were elicited through somatic current injection (1–2 nA amplitude, 1 ms duration, 50 Hz). Fluo-5F and Alexa 594 signals were collected simultaneously in linescan mode (∼600 Hz), with line ROIs encompassing both boutons. Each measurement consisted of 10 linescans repeated at 5 s intervals. After an initial 10 scans following patch equilibration (>15 min), a linescan bout was taken every 10 min for another 30 min, where drug application occurred after the 2$^{nd}$ bout. Between bouts, adjustments were made at low laser power to keep both boutons in the imaging plane. ACSF was supplemented with 0.01% bovine serum albumen during experiments involving ω-conotoxin-MVIIC to aid drug wash-out between recordings.

Analysis was performed on 10-linescan averages at each timepoint. ΔG/R peaks were determined by fitting an exponential to the fluorescence decay following the final stimulus. We also measured ΔG/R of the initial peak in the triplet stimulus by averaging fluorescence over a 10 ms window surrounding the first AP. These measurements were highly correlated with each other (Figure S7C). Furthermore, group differences in SOM+ bouton Ca transients across drug conditions were similar when using initial peaks compared to final peaks (Figure S7B). Peak extraction was performed in MATLAB and smoothed with a 3-point binomial filter for presentation. Maximum intensity image projections are displayed using the ''Red Hot'' lookup table in FIJI. Full neuronal and dendritic reconstructions were stitched together using pairwise stitching in FIJI before generation of maximum intensity projections.

## QUANTIFICATION AND STATISTICAL ANALYSIS

Data are summarized by mean ± standard error (SEM) with individual data points overlaid. Number of recordings per group are denoted in the text as n for cells and N for mice. Normality for each group was tested using Kolmorogov-Smirnov test, and group differences were assessed with parametric (Student's T test) or non-parametric tests (Wilcoxon signed rank, Holm-Sidak post-hoc test). accordingly. Data were mostly normally distributed, and paired or unpaired t-tests were used unless otherwise specified. Statistical analysis was performed using Prism (GraphPad) and reported in the results or supplemental figure legends. $^{***}p < 0.001$, $^{**}p < 0.01$, $^{*}p < 0.05$.